Veterinary and Comparative Oncology

WILEY

Veterinary and Comparative Oncology

ORIGINAL ARTICLE OPEN ACCESS

Fluvastatin Plus Dipyridamole Suppresses Canine Hemangiosarcoma Growth in Patient-Derived Xenograft Models Through Lactate Dehydrogenase-Associated Cholesterol/Lipid Metabolism

Tamami Suzuki[1] | Suzune Tanaka[1] | Keika Kishimoto[1] | Takuma Goto[1] | Jumpei Yamazaki[2,3] | Takashi Kimura[1] | Keisuke Aoshima[1,3]

[1]Laboratory of Comparative Pathology, Department of Clinical Sciences, Faculty of Veterinary Medicine, Hokkaido University, Sapporo, Hokkaido, Japan | [2]Translational Research Unit, Veterinary Teaching Hospital, Faculty of Veterinary Medicine, Hokkaido University, Sapporo, Hokkaido, Japan | [3]Cancer Research Unit, One Health Research Center, Hokkaido University, Sapporo, Hokkaido, Japan

Correspondence: Keisuke Aoshima (k-aoshima@vetmed.hokudai.ac.jp)

Received: 5 March 2026 | **Revised:** 7 July 2026 | **Accepted:** 28 July 2026

Keywords: combination | drug therapy | gene expression profiling | histones | neoplasms | neoplasm transplantation | vascular tissue

ABSTRACT

Tumour cells commonly exhibit aerobic glycolysis and produce lactate despite oxygen availability. Lactate dehydrogenase (LDH) catalyses pyruvate-lactate interconversion and regulates intracellular lactate levels. Endothelial cells also depend on glycolysis for ATP production, which prompted us to investigate LDH in canine hemangiosarcoma (HSA), a malignant endothelial tumour. We inhibited LDH with (R)-GNE-140 or sodium oxamate in two canine HSA cell lines (HU-HSA-2 and HU-HSA-3) and generated HU-HSA-3 clones with knockout of *LDHA* or *LDHB* to evaluate the effects of LDH perturbation. (R)-GNE-140 and sodium oxamate suppressed proliferation and reduced global histone lactylation levels in both cell lines. mRNA-sequencing (mRNA-seq) of (R)-GNE-140-treated HU-HSA-2 cells identified cholesterol/lipid metabolism-related gene sets among the top negatively enriched pathways. Representative cholesterol/lipid metabolism genes such as *SREBF2*, *SQLE* and *LDLR* responded differently depending on cell lines and inhibitors. (R)-GNE-140 decreased these genes in HU-HSA-2 but not HU-HSA-3, whereas sodium oxamate decreased them in HU-HSA-3 with limited effects in HU-HSA-2. In HU-HSA-3, *LDHA* and *LDHB* knockout clones decreased SREBP2 expression and reduced the number of lipid droplets. Fluvastatin, a cholesterol metabolism inhibitor, inhibited HSA cell growth in vitro but did not significantly suppress tumour growth in two HSA patient-derived xenograft (PDX) models. In contrast, combined fluvastatin and dipyridamole treatment inhibited proliferation in vitro and tumour growth in PDX models. Collectively, these results suggest a context-dependent association between LDH and cholesterol/lipid metabolism in canine HSA cell lines and provide a rationale for further evaluation of combined cholesterol pathway inhibition.

1 | Introduction

Tumour cells exhibit altered metabolism, including aerobic glycolysis (the Warburg effect), which generates abundant lactate. High lactate concentrations in the tumour microenvironment are associated with aggressive behaviour and poor prognosis, and lactate can promote tumour progression through effects on tumour and stromal tissues [1]. Lactate

Tamami Suzuki and Suzune Tanaka contributed equally to this work.

levels are regulated by lactate dehydrogenase (LDH), which catalyses the interconversion of pyruvate and lactate while regenerating NAD^+ from NADH [2]. LDH functions as a tetramer composed of LDHA and LDHB subunits, and isoform composition and subcellular localization can vary across tissues and tumours. Notably, nuclear localization of LDHA has been reported in some contexts, supporting potential non-canonical roles linking metabolism to chromatin regulation [3]. Indeed, lactate is also associated with epigenetic regulation. Histone lactylation is a lactate-derived posttranslational modification whose global level correlates with intracellular lactate concentration and can influence transcriptional programmes relevant to cancer biology [4–6].

Beyond glycolysis, tumour cells extensively reprogram lipid metabolism. Cholesterol uptake and biosynthesis support membrane biogenesis and oncogenic signalling [7], and tumour cells store excess cholesterol as cholesteryl esters within lipid droplets [8]. Nutrient-sensing pathways such as the mechanistic target of rapamycin complex 1 (mTORC1) can promote the activation of sterol regulatory element-binding proteins (SREBPs) and lipogenesis [9]. Statins inhibit HMG-CoA reductase, but their efficacy is often limited by sterol-regulated feedback mediated by SREBP2, a master transcription factor for cholesterol biosynthesis genes [10, 11]. Dipyridamole, an anti-platelet agent and vasodilator, inhibits SREBP2 maturation and can enhance the anti-tumour effect of statins in human cancers [10–12].

Canine hemangiosarcoma (HSA) is a highly malignant vascular endothelial tumour with poor prognosis. Standard treatment consists of surgical resection followed by adjuvant chemotherapy, yet the reported 2-year survival rate remains as low as 3.8% [13, 14]. Visceral HSA is frequently diagnosed at an advanced stage because metastasis is often present at diagnosis or develops shortly thereafter [13, 15]. Thus, multimodal treatment rarely achieves long-term disease control in dogs with splenic HSA [13–15]. Although molecular profiling has identified candidate therapeutic targets, no molecularly targeted therapy has been established as a standard adjuvant treatment for canine HSA [16, 17]. These limitations highlight the need to identify biological pathways that support HSA growth and progression. Given that HSA is an endothelial cell tumour and endothelial cells rely primarily on glycolysis even under aerobic conditions [18], lactate metabolism may be associated with HSA biology. However, the role of LDH in HSA remains largely unexplored.

In this study, we investigated whether LDH is involved in canine HSA biology. We first perturbed LDH using (R)-GNE-140, a dual inhibitor of LDHA and LDHB, and sodium oxamate, a pyruvate analogue and competitive LDH inhibitor, as well as LDHA/LDHB knockout in canine HSA cell lines. These analyses identified an association between LDH perturbation and cholesterol/lipid metabolism, which led us to evaluate cholesterol biosynthesis inhibition with fluvastatin in vitro and in patient-derived xenograft (PDX) models. Since statin efficacy can be limited by SREBP2-mediated feedback, we further tested fluvastatin in combination with dipyridamole to attenuate this feedback.

2 | Materials and Methods

Supporting Information includes full methods, Figure S1 and Tables S1–S5.

2.1 | Cell Culture

Two canine HSA cell lines (HU-HSA-2 and HU-HSA-3) were previously established from dogs with splenic hemangiosarcoma [6]. 293T cells were obtained from RIKEN BioResource Research Center. Cells were cultured in Dulbecco's Modified Eagle Medium (DMEM; #044-29765, FUJIFILM Wako Pure Chemical Corporation, Osaka, Japan) supplemented with 10% foetal bovine serum (FBS; #10270-106, Thermo Fisher Scientific, Waltham, Massachusetts, USA) and penicillin–streptomycin (P/S; #168-23191, FUJIFILM Wako) at 37°C with 5% CO_2.

2.2 | Cell Line Authentication Statement

No additional authentication was performed in this study. HU-HSA-2 and HU-HSA-3 cells were established and authenticated in our previous study [6]. 293T cells were authenticated in RIKEN BioResource Research Center (RCB2202).

2.3 | LDHA and LDHB Knockout Cell Generation

293T cells were transfected with lentiCRISPRv2 containing designed single guide RNAs (sgRNAs), HIV-gp and VSV-G using Lipofectamine 3000 with P3000 reagent (#L300015, Thermo Fisher Scientific) in Opti-MEM (#31985070, Thermo Fisher Scientific) according to the manufacturer's instructions. Forty-eight hours after transfection, the medium was filtered and collected as viral solutions. Selection was done with medium containing puromycin. Cells were seeded into 96-well plates at a density of 0.5 cells per well to obtain clones.

2.4 | Cell Proliferation Assay

The number of live cells was counted using Countess II (AMQAX1000, Thermo) or using Cell Counting Kit-8 (CCK-8; #343-07623, Dojindo Laboratories, Kumamoto, Japan) according to the manufacturer's instructions. Relative viability was calculated by setting control samples as 100%. KyPlot 6.0 software (KyensLab Inc., Tokyo, Japan) was used to generate survival curves [19].

2.5 | Protein Extraction and Western Blotting

SDS lysis buffer was added to cultured cells after washing with phosphate-buffered saline (PBS) twice. Protein concentrations were measured with TaKaRa BCA Protein Assay Kit (#T9300A, Takara Bio Inc., Kusatsu, Shiga, Japan). Proteins were separated on 8%–18% SDS-polyacrylamide gels. Protein-transferred membranes were blocked with 3% skim milk in Tris-buffered saline with 0.05% Tween20 (TBST) for 1 h at room temperature (RT) and incubated with primary antibodies overnight at 4°C.

Membranes were then incubated with the corresponding secondary antibodies. Antibodies used in this study are listed in Table S1.

2.6 | mRNA-Seq

HU-HSA-2 cells were treated with DMSO or 10 μM (R)-GNE-140 for 72 h in triplicate. Sequence reads were mapped to ROS_Cfam_1.0 (CanFam 4) using STAR [20], and expression levels were estimated using RSEM [21]. Differential expression analysis was performed using edgeR, and gene expression profiles were analysed by gene set enrichment analysis (GSEA) v4.1.0 [22, 23]. Gene Ontology analysis was conducted using Metascape [24].

2.7 | RNA Extraction and Reverse Transcription Quantitative Polymerase Chain Reaction (RT-qPCR)

Total RNA was extracted by using TriPure Isolation Reagent (#11667157001, Roche, Basel, Switzerland), and reverse transcription was performed using PrimeScript Reverse Transcriptase II (#2690A, Takara Bio) according to the manufacturer's instructions. qPCR was performed using the cDNAs and primers listed in Table S2. Results were normalised based on the geometric mean of reference genes, which were selected from seven potential internal controls (*RPL32, RPL13A, TBP, YWHAZ, HMBS, B2M* and *ACTB*) using geNorm software [25]. Selected reference genes for each experiment are listed in Table S3.

2.8 | Lipid Droplet Staining

For visualisation of lipid droplets, scramble, *LDHA* and *LDHB* knockout HU-HSA-3 clones were fixed with 4% paraformaldehyde for 7.5 min at RT, and stained with Lipi-Green (#LD02, Dojindo) diluted in PBS according to the manufacturer's instructions. Images were acquired using a confocal laser microscope (LSM 800, Carl Zeiss, Oberkochen, Germany). For quantification of lipid droplets, 30 confocal images (one cell per image) were analysed for each clone and quantified using ImageJ [26]. Individual cells were manually outlined as regions of interest. Images were converted to 8-bit and thresholded using Li's method (dark background) [27]. A binary mask was generated, droplets were separated using the watershed algorithm, and particles were quantified with Analyze Particles (size: 0.0005–0.10; circularity: 0–1.00).

2.9 | Animal Studies

All mouse experiments were performed under the guidelines (protocol number: 20-0083, 21-0062, 25-0062). Female 4- to 8-week-old KSN/Slc mice (*Mus musculus*, Japan SLC Inc.) were used for experiments. PDX tumour fragments were transplanted subcutaneously in the right flank of mice. Tumour volumes were calculated using the formula: volume = (length × width^2)/2. When the tumour volume reached 100 mm^3, mice were allocated to groups, and treatments were started. For HU-HSAPDX-3 and HU-HSAPDX-5, mice received intraperitoneal fluvastatin (30 mg/kg) or PBS every other day for up to 30 days or until tumours reached 1 cm^3. For HU-HSAPDX-6 and HU-HSAPDX-7, mice received oral fluvastatin (50 mg/kg) and/or intraperitoneal dipyridamole (120 mg/kg) daily for 2 weeks. PBS and dipyridamole solvent served as vehicle controls. Mice were euthanized with CO_2 at the end of treatment.

2.10 | Statistical Analysis

Statistical analyses were performed with Microsoft Excel (version 2019) and R software (version 4.2.0). For in vivo experiments, tumour growth was analysed with two-way ANOVA. Cell proliferation was analysed with two-way ANOVA and Dunnett's test. Statistical comparisons for lipid droplet quantification and qPCR among the three groups (scramble, LDHA knockout and LDHB knockout clones) were performed using the Kruskal-Wallis test. Dunn's multiple comparison test with Benjamini–Hochberg correction was subsequently used for post hoc analysis.

3 | Results

3.1 | LDH Is Associated With Cholesterol/Lipid Metabolic Pathways in HU-HSA-2 and HU-HSA-3 Cell Lines

To investigate the role of LDH activity in HSA cells, we evaluated the effects of (R)-GNE-140, a dual inhibitor of LDHA and LDHB, on cell proliferation and global histone lactylation levels in two HSA cell lines (HU-HSA-2 and HU-HSA-3). Given that lactate can serve as a substrate for histone lactylation, we monitored global histone lactylation levels as a surrogate readout of the downstream effect of LDH inhibition. (R)-GNE-140 significantly suppressed proliferation of both HU-HSA-2 and HU-HSA-3 in vitro (Figure 1A). In HU-HSA-2, LDHA and LDHB protein levels were modestly increased after (R)-GNE-140 treatment, possibly reflecting compensatory upregulation, whereas no obvious change was observed in HU-HSA-3 (Figure 1B). Global histone lactylation levels were reduced in both cell lines (Figure 1B). Next, to identify gene expression changes associated with LDH inhibition, we performed mRNA-seq on HU-HSA-2 cells treated with (R)-GNE-140 because HU-HSA-2 showed a more pronounced anti-areproliferative response. GSEA revealed that multiple cholesterol/lipid metabolism gene sets were among the top 10 negatively enriched pathways (Figure 1C,D), and Gene Ontology enrichment analysis using Metascape of significantly downregulated genes ($\geq$2-fold; $q < 0.05$) similarly highlighted terms related to cholesterol/lipid metabolism (Figure 1E). Furthermore, downregulation of representative cholesterol/lipid metabolism genes was validated by RT–qPCR in HU-HSA-2 (Figure 1F). In contrast, (R)-GNE-140 did not significantly reduce the expression levels of representative cholesterol/lipid metabolism genes in HU-HSA-3 (Figure 1F).

Alternatively, sodium oxamate, a pyruvate analogue and competitive inhibitor of LDH, suppressed the proliferation of both HU-HSA-2 and HU-HSA-3 in vitro in a dose-dependent manner (Figure 2A). Although LDHA and LDHB protein levels were not altered, sodium oxamate decreased global histone lactylation levels in both cell lines (Figure 2B). The expression levels of representative

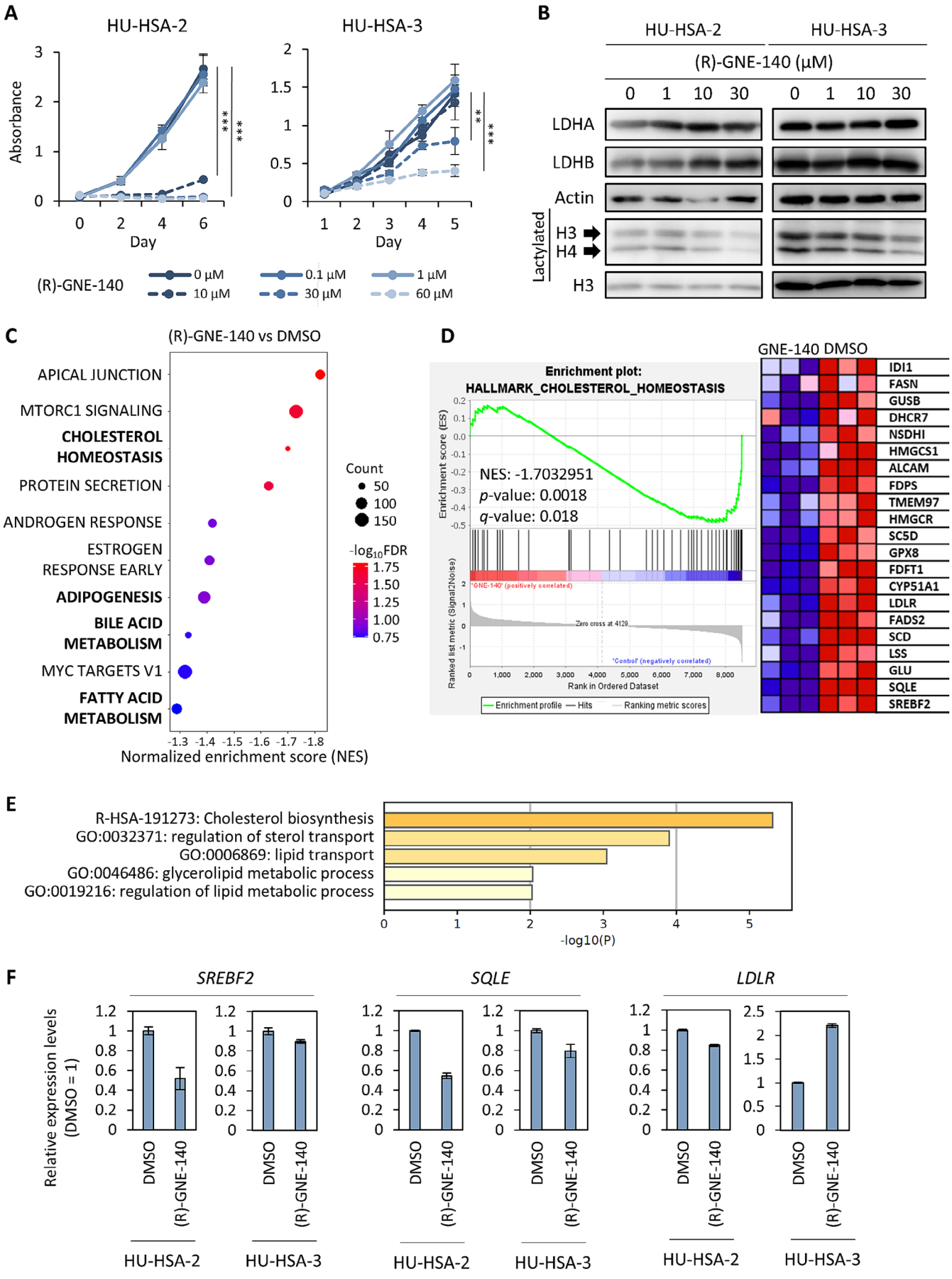

FIGURE 1 | Legend on next page.

FIGURE 1 | (R)-GNE-140 represses HSA cell proliferation and is associated with suppression of cholesterol/lipid metabolism in HU-HSA-2. (A) Cell proliferation curves of HU-HSA-2 and HU-HSA-3 treated with indicated concentrations of (R)-GNE-140. $^{**}p < 0.01$, $^{***}p < 0.001$. Dunnett's test. Data are presented as average ± SD ($n = 3$). (B) Western blotting analysis for HU-HSA-2 and HU-HSA-3 cells 48 h after treatment with indicated concentrations of (R)-GNE-140 (0 μM is the DMSO control). (C–E) GSEA and Metascape analyses of HU-HSA-2 cells treated with 10 μM (R)-GNE-140 for 72 h compared to DMSO controls. (C) Dot plot of the top 10 negatively enriched pathways in GSEA. (D) GSEA enrichment plot (left) and heat map (right) of HALLMARK_CHOLESTEROL_HOMEOSTASIS gene set. (E) Gene Ontology enrichment analysis results generated using Metascape. (F) RT-qPCR analysis of representative cholesterol/lipid metabolism genes in HU-HSA-2 cells treated with 10 μM (R)-GNE-140 or DMSO for 72 h and in HU-HSA-3 cells treated with DMSO or 30 μM (R)-GNE-140 for 48 h. *B2M* and *TBP* were used in HU-HSA-2, and *RPL32* and *HMBS* were used in HU-HSA-3 as reference genes. Data are shown relative to DMSO controls (DMSO = 1) and as average ± SD ($n = 3$).

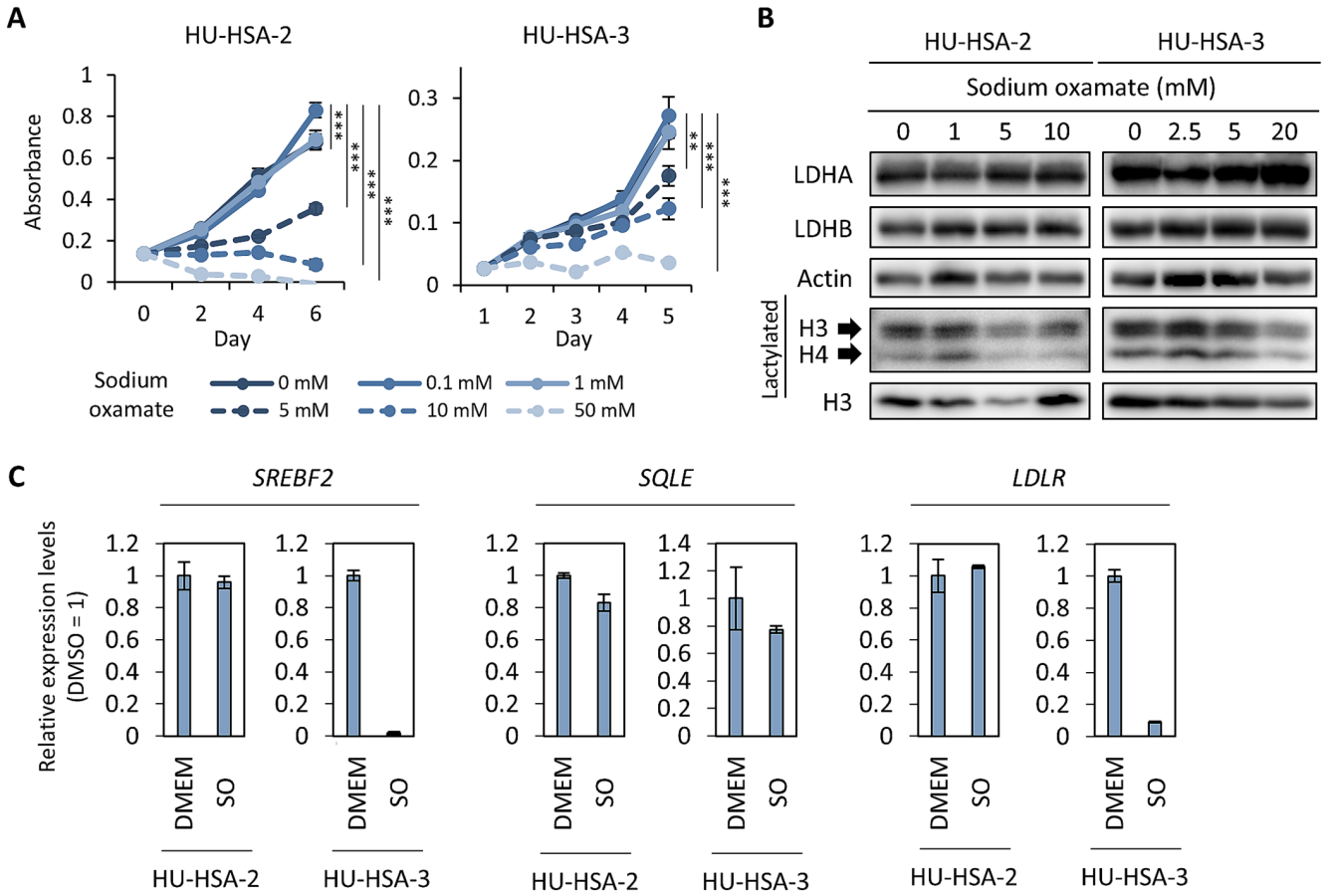

FIGURE 2 | Sodium oxamate represses HSA cell proliferation and is associated with suppression of cholesterol/lipid metabolism in HU-HSA-3. (A) Cell proliferation curves of HU-HSA-2 and HU-HSA-3 treated with indicated concentrations of sodium oxamate. $^{**}p < 0.01$, $^{***}p < 0.001$. Dunnett's test. Data are presented as average ± SD ($n = 3$). (B) Western blotting analysis for HU-HSA-2 and HU-HSA-3 cells 48 h after treatment with indicated concentrations of sodium oxamate (0 mM is the DMEM control). (C) RT-qPCR analysis of representative cholesterol/lipid metabolism genes in HU-HSA-2 and HU-HSA-3 cells treated with 10 mM sodium oxamate (SO) or DMEM (control) for 48 h. *RPL32* and *YWHAZ* were used as reference genes. Data are shown relative to DMEM controls (DMEM = 1) and as average ± SD ($n = 3$).

cholesterol/lipid metabolism genes were markedly reduced in HU-HSA-3, whereas changes in HU-HSA-2 were limited (Figure 2C).

To directly assess the contributions of LDHA and LDHB to cholesterol/lipid metabolism gene expression, we generated LDHA- and LDHB-knockout HU-HSA-3 clones (LDHA KO #1–4, LDHB KO #1–4, Figure 3A). The expression levels of SREBP2 (*SREBF2*), a key regulator of cholesterol homeostasis, were reduced in both LDHA- and LDHB-knockout clones (Figure 3A). Global histone lactylation levels were decreased in LDHA-knockout clones but were not consistently altered across LDHB-knockout clones (Figure 3A). Cholesterol/lipid metabolism genes were broadly downregulated in LDHA-knockout clones, whereas LDHB-knockout clones showed variable effects (Figure 3B). To assess the functional effects on intracellular lipid storage, we stained and quantified lipid droplets in HU-HSA-3 knockout clones. Both *LDHA* and *LDHB* knockout clones showed reduced lipid droplet numbers compared to scramble controls (Figure 4A–C).

Together, these results suggest that LDH inhibition and genetic loss are associated with changes in cholesterol/lipid metabolism gene expression, and that responsiveness to LDH inhibitors differs between HU-HSA-2 and HU-HSA-3 cell lines.

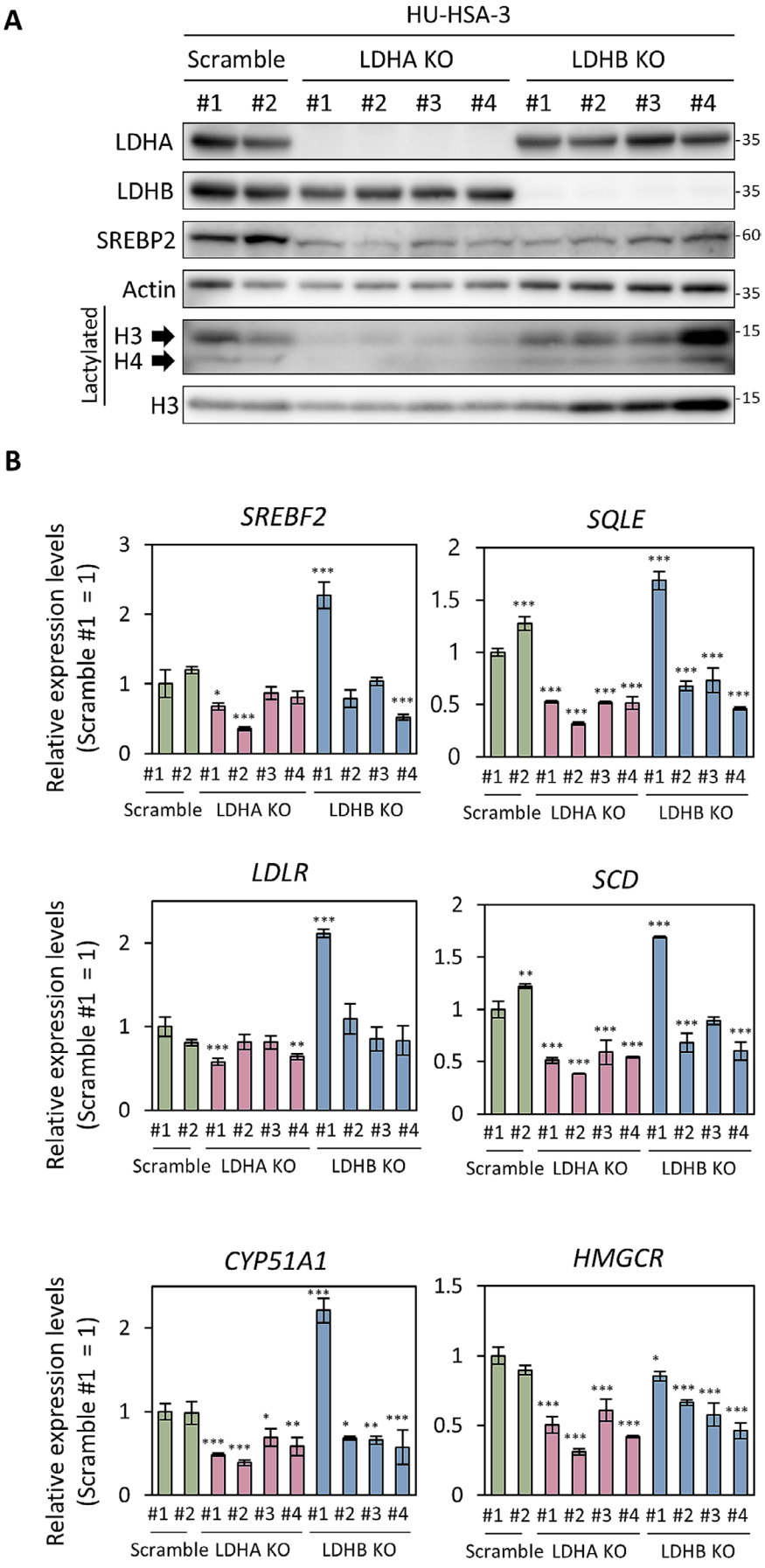

FIGURE 3 | Legend on next page.

FIGURE 3 | *LDHA* knockout was associated with downregulation of cholesterol/lipid metabolism genes. (A) Western blot analysis for scramble (control), *LDHA* knockout (LDHA KO) and *LDHB* knockout (LDHB KO) HU-HSA-3 clones. (B) RT-qPCR analysis of cholesterol metabolism/lipid metabolism genes in HU-HSA-3 clones. Gene expression was normalised to Scramble #1. Data are presented as average ± SD ($n = 3$). *HMBS* and *B2M* were used as reference genes. *$p < 0.05$, **$p < 0.01$, ***$p < 0.001$. Dunnett's test.

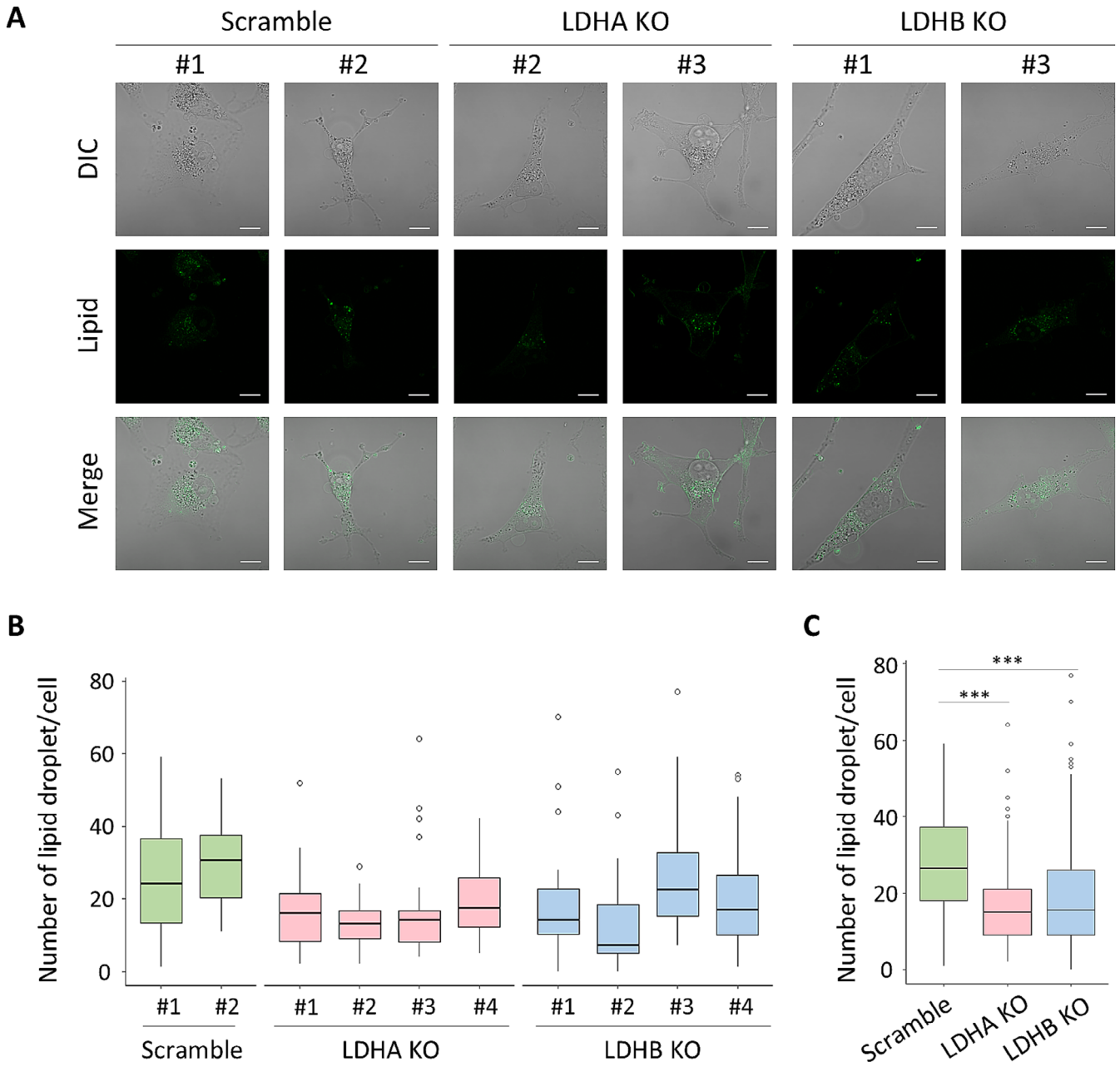

FIGURE 4 | LDH knockout suppresses lipid droplet synthesis. (A) Representative images of HU-HSA-3 scramble control clones (#1 and #2), LDHA KO clones (#2 and #3) and LDHB KO clones (#1 and #3). Images show differential interference contrast (DIC), lipid droplet staining (Lipid) and merged images. Scale bars = 10 μm. (B) Box plots showing the number of lipid droplets per cell in individual clones (30 cells per clone). (C) Box plots showing the number of lipid droplets per cell in the pooled populations. (Scramble, $n = 60$; LDHA KO, $n = 120$; LDHB KO, $n = 120$). ***$p < 0.001$. Kruskal–Wallis test followed by Dunn's multiple comparisons test.

3.2 | Statins Inhibit HU-HSA Cell Proliferation in Vitro, and Fluvastatin Plus Dipyridamole Suppresses HSA PDX Tumour Growth

Given the observed association between LDH perturbation and cholesterol/lipid metabolism, together with reduced SREBP2 (*SREBF2*) levels, we assessed whether inhibition of the cholesterol biosynthesis pathway with statins suppresses HSA cell growth. Fluvastatin and rosuvastatin, HMG-CoA reductase inhibitors, significantly reduced cell growth of both HU-HSA-2 and HU-HSA-3 cells in vitro (Figure 5A,B). Fluvastatin increased cleaved caspase-3 levels, an apoptosis marker, in both

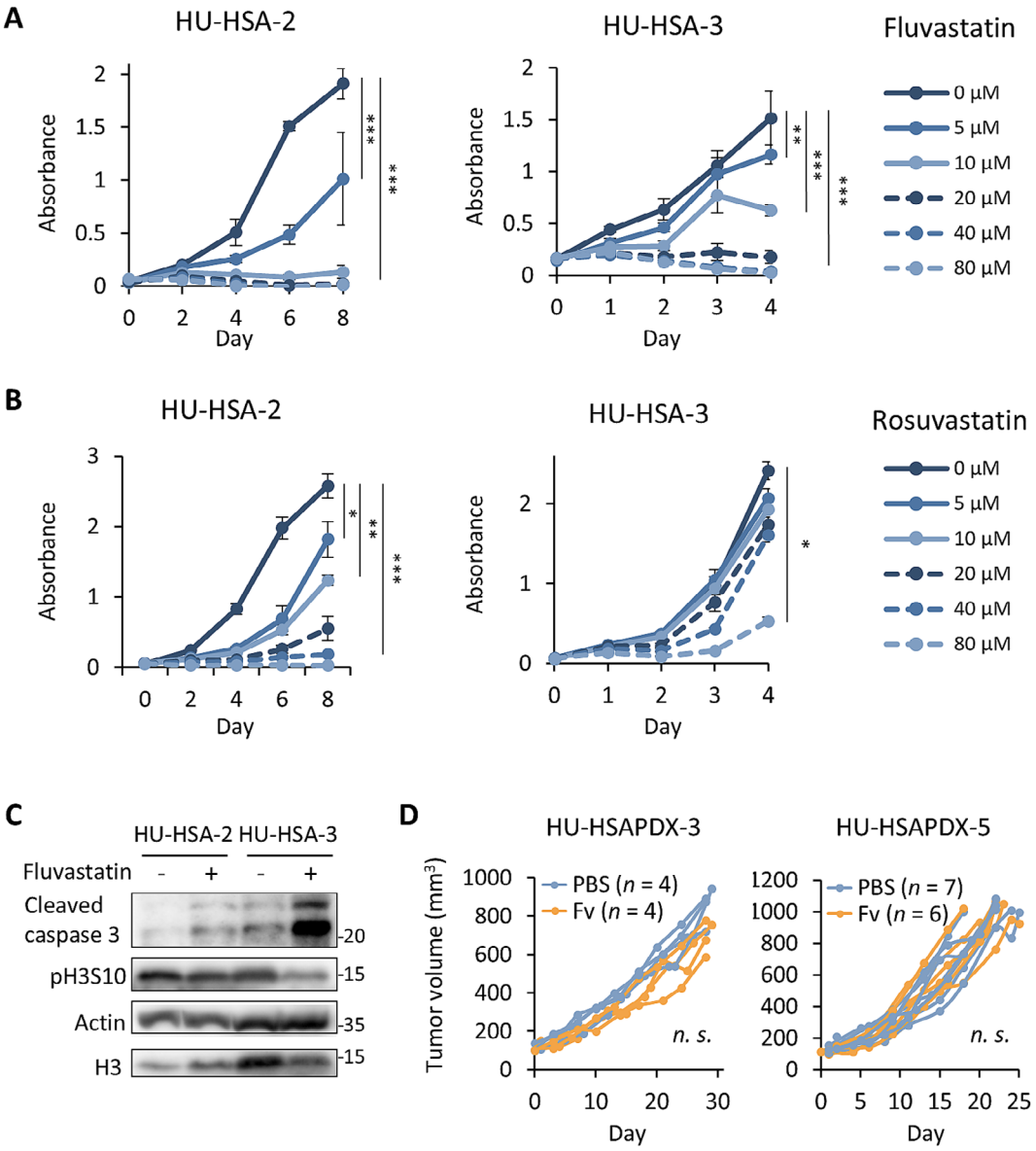

FIGURE 5 | Statins inhibit HSA cell proliferation in vitro. (A, B) Cell proliferation curves of HU-HSA-2 and HU-HSA-3 treated with indicated concentrations of fluvastatin (A) or rosuvastatin (B). $*p<0.05$, $**p<0.01$, $***p<0.001$. Dunnett's test. Data are presented as mean ± SD ($n=3$). (C) Western blot analysis for HU-HSA-2 and HU-HSA-3 treated with DMSO or 10 μM fluvastatin for 48 h. (D) Tumour growth curves of HU-HSAPDX-3 and HU-HSAPDX-5 treated with PBS or fluvastatin (Fv) intraperitoneally. *n.s.*, not significant. Two-way ANOVA.

cell lines, and it reduced phospho-histone H3 (pH3S10) levels in HU-HSA-3 (Figure 5C). To assess its anti-tumour activity in vivo, we treated canine HSA PDX models (HU-HSAPDX-3 and HU-HSAPDX-5) with fluvastatin intraperitoneally; however, no statistically significant suppression of tumour growth was observed in either model (Figure 5D).

To enhance the inhibitory effect on the cholesterol biosynthesis pathway, we evaluated fluvastatin in combination with dipyridamole. Dipyridamole reduced HU-HSA-2 and HU-HSA-3 cell viability in vitro in the micromolar range (Figure 6A), and co-treatment with fluvastatin produced overall additive effects in both cell lines (ZIP synergy score: 7.656 ± 1.2 for HU-HSA-2 and 4.236 ± 0.96 for HU-HSA-3; Figure 6B). Finally, we treated canine HSA PDX models (HU-HSAPDX-6 and HU-HSAPDX-7) with fluvastatin (p.o.) and/or dipyridamole (i.p.). While dipyridamole monotherapy showed modest tumour growth inhibition, combination treatment resulted in greater tumour growth reduction in both PDX models (Figure 6C). Body weight remained stable across treatment groups (Figure 6D).

These results indicate that although fluvastatin monotherapy showed limited activity in vivo, co-treatment with dipyridamole could enhance tumour growth inhibition in PDX models.

4 | Discussion

Given that canine HSA remains difficult to control, identifying biological pathways that support tumour growth and dissemination is important for developing new therapeutic strategies. Our results support a functional association

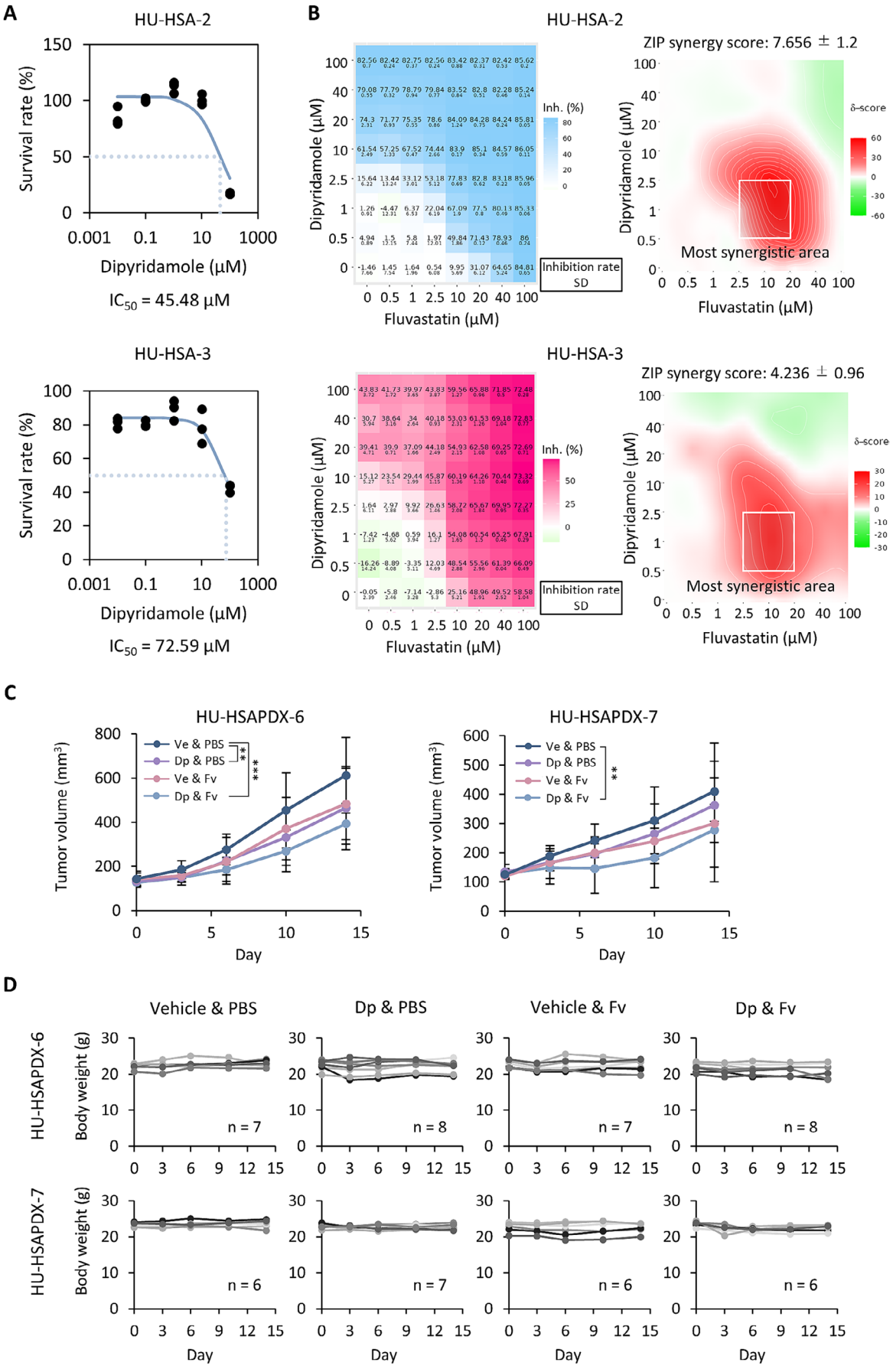

FIGURE 6 | Legend on next page.

FIGURE 6 | Co-treatment with fluvastatin and dipyridamole suppresses PDX tumour growth. (A) Survival curves and IC_{50} values for HU-HSA-2 (top) and HU-HSA-3 (bottom) cells treated with dipyridamole for 48 h. (B) Inhibition matrices (left) and synergy maps (right) for HU-HSA-2 (top) and HU-HSA-3 (bottom) cells treated with dipyridamole and fluvastatin. Values in the inhibition matrices are presented as mean ± SD ($n = 3$). Synergy was evaluated using the ZIP model. ZIP synergy scores are shown. The most synergistic area is boxed. (C) Tumour growth curves of HU-HSAPDX-6 and HU-HSAPDX-7 treated with vehicle (Ve) or dipyridamole (Dp) in combination with PBS or fluvastatin (Fv). $^{**}p < 0.01$, $^{***}p < 0.001$. Two-way ANOVA. Data are presented as mean ± SD ($n = 6$–8 per group). (D) Body weight plots of individual mice in the co-treatment experiments for HU-HSAPDX-6 and HU-HSAPDX-7.

between LDH and cholesterol/lipid metabolism in HSA cells and suggest that LDH-associated cholesterol/lipid metabolism may represent a candidate therapeutic target, particularly when SREBP2-mediated sterol-regulated feedback is concurrently targeted.

Based on its canonical role, LDH perturbation would be expected primarily to affect lactate-associated metabolism and glycolysis. It was therefore notable that transcriptome profiling of (R)-GNE-140 treated HU-HSA-2 cells identified cholesterol/lipid metabolism gene sets among the most negatively enriched pathways. However, our results indicate that the relationship between LDH perturbation and cholesterol/lipid metabolism is context dependent. In HU-HSA-2, (R)-GNE-140 suppressed representative cholesterol/lipid metabolism genes, whereas (R)-GNE-140 did not comparably suppress them in HU-HSA-3. Conversely, sodium oxamate reduced cholesterol/lipid metabolism gene expression in HU-HSA-3 but not HU-HSA-2. This difference may reflect biological heterogeneity at both the inter-tumour level (patient-to-patient differences) and the intra-tumour level (distinct subpopulations within a tumour tissue) [28]. Our knockout experiments further suggest that LDHA plays an important role in regulating cholesterol/lipid metabolism gene expression in HU-HSA-3. *LDHA* knockout clones showed consistent reductions in their expressions, whereas *LDHB* knockout clones showed variable effects. In parallel, global histone lactylation decreased robustly in LDHA knockout clones but was not consistently altered across LDHB knockout clones. These findings suggest that cholesterol/lipid metabolism gene regulation is more tightly coupled to LDHA than to LDHB alone, potentially reflecting isoform-specific substrate preferences and compartmentalization (e.g., nuclear LDHA and mitochondrial-associated LDHB in some contexts) [2, 3, 29]. However, *LDHB* knockout clones also showed reduced SREBP2 protein levels and decreased lipid droplet numbers. This suggests that LDHB also contributes to cholesterol biosynthesis, possibly through mechanisms different from LDHA. To define how broadly this LDH-cholesterol/lipid metabolism relationship applies to HSA pathogenesis and to fully understand its mechanism, additional HSA models such as other primary cell lines, cell line-derived xenografts and PDX models, should be studied.

Mechanistically, LDH inhibition may modulate cholesterol/lipid metabolism through coupled redox control and lactate-linked chromatin regulation. The LDH reaction couples pyruvate-lactate interconversion to the regeneration of cytosolic NAD^+ from NADH [30, 31]. LDH inhibition can promote reductive stress (an increased cytosolic NADH/NAD^+ ratio), which can constrain glycolytic flux and downstream acetyl-CoA production [30, 31]. These metabolic changes potentially attenuate nutrient-sensing pathways such as the mTORC1 pathway, which in turn suppresses SREBP activation and the subsequent transcriptional programme for cholesterol biosynthesis [9, 32]. Consistent with this, our HU-HSA-2 transcriptome analysis showed coordinated downregulation of cholesterol/lipid gene sets with reduced mTORC1 signalling following (R)-GNE-140 exposure. In parallel, reduced intracellular lactate availability may limit the substrate for histone lactylation [4, 6]. The concurrent reduction in global histone lactylation and lipid droplet accumulation observed in LDHA-knockout HU-HSA-3 cells suggests the possibility that histone lactylation contributes to the transcriptional maintenance of cholesterol/lipid pathways. Establishing a direct causal link, however, requires demonstrating that lactylation marks are specifically enriched at the promoters or other regulatory regions of these metabolic genes.

The inhibitory effects on LDH exerted by small-molecule inhibitors and genetic knockout should be interpreted with caution. (R)-GNE-140 is a potent small-molecule LDH inhibitor whose binding is reported to be NADH-dependent, likely reflecting preferential engagement of the NADH-bound enzyme state [33]. By contrast, sodium oxamate is a pyruvate analogue that competitively inhibits the substrate-binding site on the LDH-NADH complex [34]. Given that sodium oxamate competes with intracellular pyruvate, its efficacy is expected to vary according to pyruvate abundance and the broader metabolic state. Specifically, HU-HSA-3 cells rely more heavily on glucose for ATP production than HU-HSA-2 [6]. Consequently, sodium oxamate might perturb pyruvate metabolism and redox homeostasis beyond simple LDH inhibition, potentially contributing to the observed decrease in cholesterol/lipid gene expression in HU-HSA-3 cells [34, 35]. Furthermore, knocking out either LDHA or LDHB can induce compensatory remodelling of LDH tetramers, whereas small-molecule inhibitors suppress the activity of all LDH tetramers regardless of their subunit composition [36, 37]. Collectively, while these factors have to be carefully taken into account, our data indicate an association between LDH and cholesterol/lipid metabolism.

The enhanced anti-tumour activity of the fluvastatin-dipyridamole combination in our PDX models is consistent with prior human cancer studies [10, 11]. Statin-mediated inhibition of HMG-CoA reductase can activate an SREBP2-driven sterol-regulated feedback response that limits statin cytotoxicity, whereas dipyridamole attenuates this response [10, 11]. In both co-treated HSA PDX models (HU-HSAPDX-6 and HU-HSAPDX-7), tumour growth was significantly delayed compared with either fluvastatin or dipyridamole monotherapy; however, co-treatment did not induce overt tumour regression. This suggests that fluvastatin-dipyridamole co-treatment might be insufficient to shrink established tumours at least under the tested conditions. Nonetheless, a cytostatic effect may still have

clinical utility in canine HSA, in which metastasis often occurs prior to or shortly after diagnosis, and systemic therapy is commonly conducted following surgical removal of primary tumours [38, 39]. Although doxorubicin-based adjuvant therapy is associated with longer survival than surgery alone, overall outcomes remain poor [40]. Accordingly, additional systemic strategies that delay metastatic/disseminating progression may improve patient prognosis. Therefore, it may be more clinically relevant to evaluate the efficacy of fluvastatin-dipyridamole co-treatment in metastatic or disseminating conditions. To this end, the development of HSA models such as cell-line-derived xenografts and PDX models capable of metastasis or dissemination is essential for future preclinical evaluations.

Several limitations should be considered. The LDH inhibitor experiments used high micromolar concentrations of (R)-GNE-140 and millimolar concentrations of sodium oxamate; therefore, these experiments should be interpreted as mechanistic perturbation studies. Fluvastatin and dipyridamole also inhibited HSA cell growth at micromolar concentrations in vitro, and the combination delayed PDX tumour growth only at relatively high doses. To identify an appropriate therapeutic window in dogs, further canine pharmacokinetic, pharmacodynamic and safety studies are required.

In conclusion, we identified a functional link between LDH and cholesterol/lipid metabolism in canine HSA cell lines and demonstrated that fluvastatin-dipyridamole co-treatment significantly delayed tumour growth in HSA PDX models. Further studies are warranted to elucidate the mechanisms by which LDH regulates transcription of genes involved in cholesterol/lipid metabolism and to define the clinical potential of combined statin-dipyridamole therapy.

Author Contributions

T.S., S.T. and K.A. designed the research. K.A. conceived and supervised the project. T.S. and S.T. performed most experiments. T.S., S.T., K.K., T.G. and K.A. performed the dual-drug treatment experiments. K.A. conducted the bioinformatic analyses. T.S. and K.A. acquired funding. T.S., S.T. and K.A. wrote the original draft. All authors reviewed and edited the manuscript.

Acknowledgements

We thank Dr. Hironobu Yasui (Faculty of Veterinary Medicine, Hokkaido University) for helpful advice and constructive discussions. We are grateful to Drs Kenji Hosoya, Sangho Kim and Ryohei Kinoshita (Veterinary Teaching Hospital, Faculty of Veterinary Medicine, Hokkaido University) for providing patient samples, and to all members of the Laboratory of Comparative Pathology (Faculty of Veterinary Medicine, Hokkaido University) for helpful discussions, encouragement and support. We sincerely thank the canine patients whose tumour tissues were used to generate cell lines and patient-derived xenograft models for this study, and we are deeply grateful to their owners for their generous cooperation in supporting this research. We used OpenAI ChatGPT (model 5.2 Pro) and Google Gemini 2.5 Pro for English proofreading and methodological suggestions. All outputs were reviewed and edited by the authors. No AI-generated data were used.

Funding

This study was supported by the Japan Society for the Promotion of Science (JSPS) KAKENHI Grant-in-Aid for Scientific Research (C) 22K06020 (K.A.), Grant-in-Aid for Scientific Research (B) 25K02164 (K.A.) and Grant-in-Aid for JSPS Research Fellows 23KJ0056 (T.S.); the Clinical Research Promotion Research Grant, Faculty of Veterinary Medicine, Hokkaido University (K.A.); and donations from the general public.

Conflicts of Interest

The authors declare no conflicts of interest.

Data Availability Statement

mRNA-seq data are publicly available in the Gene Expression Omnibus (GEO) under accession GSE314239. All noncommercially available new materials, including constructs, cell lines and PDX models, that Hokkaido University has the right to provide will be made available to nonprofit or academic requesters upon completion of a standard material transfer agreement. Requests for materials should be addressed to K.A. (k-aoshima@vetmed.hokudai.ac.jp).

References

1. S. Walenta and W. F. Mueller-Klieser, "Lactate: Mirror and Motor of Tumor Malignancy," *Seminars in Radiation Oncology* 14, no. 3 (2004): 267–274.

2. J. R. Doherty and J. L. Cleveland, "Targeting Lactate Metabolism for Cancer Therapeutics," *Journal of Clinical Investigation* 123, no. 9 (2013): 3685–3692.

3. Y. Liu, J. Z. Guo, Y. Liu, et al., "Nuclear Lactate Dehydrogenase A Senses ROS to Produce α-Hydroxybutyrate for HPV-Induced Cervical Tumor Growth," *Nature Communications* 9, no. 1 (2018): 4429.

4. D. Zhang, Z. Tang, H. Huang, et al., "Metabolic Regulation of Gene Expression by Histone Lactylation," *Nature* 574, no. 7779 (2019): 575–580.

5. J. Yu, P. Chai, M. Xie, et al., "Histone Lactylation Drives Oncogenesis by Facilitating m6A Reader Protein YTHDF2 Expression in Ocular Melanoma," *Genome Biology* 22, no. 1 (2021): 85.

6. T. Suzuki, K. Heishima, J. Yamazaki, et al., "Lysine Lactylation Regulates ATF4-Mediated Stress Responses Under Glucose Starvation in Canine Hemangiosarcoma," *Frontiers in Veterinary Science* 13 (2026): 1734339.

7. F. Guillaumond, G. Bidaut, M. Ouaissi, et al., "Cholesterol Uptake Disruption, in Association With Chemotherapy, Is a Promising Combined Metabolic Therapy for Pancreatic Adenocarcinoma," *Proceedings of the National Academy of Sciences of the United States of America* 112, no. 8 (2015): 2473–2478.

8. J. Li, D. Gu, S. S. Y. Lee, et al., "Abrogating Cholesterol Esterification Suppresses Growth and Metastasis of Pancreatic Cancer," *Oncogene* 35, no. 50 (2016): 6378–6388.

9. T. Porstmann, C. R. Santos, B. Griffiths, et al., "SREBP Activity Is Regulated by mTORC1 and Contributes to Akt-Dependent Cell Growth," *Cell Metabolism* 8, no. 3 (2008): 224–236.

10. J. Longo, P. J. Mullen, R. Yu, et al., "An Actionable Sterol-Regulated Feedback Loop Modulates Statin Sensitivity in Prostate Cancer," *Molecular Metabolism* 25 (2019): 119–130.

11. J. Longo, A. A. Pandyra, P. Stachura, M. D. Minden, A. D. Schimmer, and L. Z. Penn, "Cyclic AMP-Hydrolyzing Phosphodiesterase Inhibitors Potentiate Statin-Induced Cancer Cell Death," *Molecular Oncology* 14, no. 10 (2020): 2533–2545.

12. A. Pandyra, P. J. Mullen, M. Kalkat, et al., "Immediate Utility of Two Approved Agents to Target Both the Metabolic Mevalonate Pathway and Its Restorative Feedback Loop," *Cancer Research* 74, no. 17 (2014): 4772–4782.

13. C. A. Clifford, A. J. Mackin, and C. J. Henry, "Treatment of Canine Hemangiosarcoma: 2000 and Beyond," *Journal of Veterinary Internal Medicine* 14, no. 5 (2000): 479–485.

14. K. M. Wendelburg, L. L. Price, K. E. Burgess, J. A. Lyons, F. H. Lew, and J. Berg, "Survival Time of Dogs With Splenic Hemangiosarcoma Treated by Splenectomy With or Without Adjuvant Chemotherapy: 208 Cases (2001–2012)," *Journal of the American Veterinary Medical Association* 247, no. 4 (2015): 393–403.

15. A. B. De Nardi, C. de Oliveira Massoco Salles Gomes, C. E. Fonseca-Alves, et al., "Diagnosis, Prognosis, and Treatment of Canine Hemangiosarcoma: A Review Based on a Consensus Organized by the Brazilian Association of Veterinary Oncology, ABROVET," *Cancers* 15, no. 7 (2023): 2025.

16. K. M. Kapturska and A. Pawlak, "New Molecular Targets in Canine Hemangiosarcoma—Comparative Review and Future of the Precision Medicine," *Veterinary and Comparative Oncology* 21, no. 3 (2023): 357–377.

17. P. A. B. Pimentel, A. Giuliano, P. M. Bęczkowski, and R. D. S. Horta, "Molecular Profile of Canine Hemangiosarcoma and Potential Novel Therapeutic Targets," *Veterinary Sciences* 10, no. 6 (2023): 387.

18. K. De Bock, M. Georgiadou, S. Schoors, et al., "Role of PFKFB3-Driven Glycolysis in Vessel Sprouting," *Cell* 154, no. 3 (2013): 651–663.

19. K. Yoshioka, "KyPlot—A User-Oriented Tool for Statistical Data Analysis and Visualization," *Computational Statistics* 17, no. 3 (2002): 425–437.

20. A. Dobin, C. A. Davis, F. Schlesinger, et al., "STAR: Ultrafast Universal Rna-Seq Aligner," *Bioinformatics* 29, no. 1 (2013): 15–21.

21. B. Li and C. N. Dewey, "RSEM: Accurate Transcript Quantification From RNA-Seq Data With or Without a Reference Genome," *BMC Bioinformatics* 12, no. 1 (2011): 323.

22. M. D. Robinson, D. J. McCarthy, and G. K. Smyth, "edgeR: A Bioconductor Package for Differential Expression Analysis of Digital Gene Expression Data," *Bioinformatics* 26, no. 1 (2010): 139–140.

23. A. Subramanian, P. Tamayo, V. K. Mootha, et al., "Gene Set Enrichment Analysis: A Knowledge-Based Approach for Interpreting Genome-Wide Expression Profiles," *Proceedings of the National Academy of Sciences of the United States of America* 102, no. 43 (2005): 15545–15550.

24. Y. Zhou, B. Zhou, L. Pache, et al., "Metascape Provides a Biologist-Oriented Resource for the Analysis of Systems-Level Datasets," *Nature Communications* 10, no. 1 (2019): 1523.

25. J. Vandesompele, K. De Preter, F. Pattyn, et al., "Accurate Normalization of Real-Time Quantitative RT-PCR Data by Geometric Averaging of Multiple Internal Control Genes," *Genome Biology* 3 (2002): research0034.

26. C. A. Schneider, W. S. Rasband, and K. W. Eliceiri, "NIH Image to ImageJ: 25 Years of Image Analysis," *Nature Methods* 9, no. 7 (2012): 671–675.

27. C. H. Li and C. K. Lee, "Minimum Cross Entropy Thresholding," *Pattern Recognition* 26, no. 4 (1993): 617–625.

28. Z. Xiao, Z. Dai, and J. W. Locasale, "Metabolic Landscape of the Tumor Microenvironment at Single Cell Resolution," *Nature Communications* 10, no. 1 (2019): 3763.

29. Y. J. Chen, N. G. Mahieu, X. Huang, et al., "Lactate Metabolism Is Associated With Mammalian Mitochondria," *Nature Chemical Biology* 12, no. 11 (2016): 937–943.

30. M. V. Liberti and J. W. Locasale, "The Warburg Effect: How Does It Benefit Cancer Cells?," *Trends in Biochemical Sciences* 41, no. 3 (2016): 211–218.

31. M. G. Vander Heiden, L. C. Cantley, and C. B. Thompson, "Understanding the Warburg Effect: The Metabolic Requirements of Cell Proliferation," *Science* 324, no. 5930 (2009): 1029–1033.

32. T. R. Peterson, S. S. Sengupta, T. E. Harris, et al., "mTOR Complex 1 Regulates Lipin 1 Localization to Control the SREBP Pathway," *Cell* 146, no. 3 (2011): 408–420.

33. A. Boudreau, H. E. Purkey, A. Hitz, et al., "Metabolic Plasticity Underpins Innate and Acquired Resistance to LDHA Inhibition," *Nature Chemical Biology* 12, no. 10 (2016): 779–786.

34. N. G. Bennett and H. Gutfreund, "The Kinetics of the Interconversion of Intermediates of the Reaction of Pig Muscle Lactate Dehydrogenase With Oxidized Nicotinamide-Adenine Dinucleotide and Lactate," *Biochemical Journal* 135 (1973): 81–85.

35. R. Moreno-Sánchez, Á. Marín-Hernández, I. Del Mazo-Monsalvo, E. Saavedra, and S. Rodríguez-Enríquez, "Assessment of the Low Inhibitory Specificity of Oxamate, Aminooxyacetate and Dichloroacetate on Cancer Energy Metabolism," *Biochimica et Biophysica Acta, General Subjects* 1861, no. 1 (2017): 3221–3236.

36. M. Ždralević, A. Brand, L. Di Ianni, et al., "Double Genetic Disruption of Lactate Dehydrogenases A and B Is Required to Ablate the "Warburg Effect" Restricting Tumor Growth to Oxidative Metabolism," *Journal of Biological Chemistry* 293, no. 41 (2018): 15947–15961.

37. X. Chen, L. Liu, S. Kang, J. R. Gnanaprakasam, and R. Wang, "The Lactate Dehydrogenase (LDH) Isoenzyme Spectrum Enables Optimally Controlling T Cell Glycolysis and Differentiation," *Science Advances* 9, no. 12 (2023): eadd9554.

38. P. F. Favaro, S. D. Stewart, B. R. McDonald, et al., "Feasibility of Circulating Tumor DNA Analysis in Dogs With Naturally Occurring Malignant and Benign Splenic Lesions," *Scientific Reports* 12, no. 1 (2022): 6337.

39. A. N. Smith, "Hemangiosarcoma in Dogs and Cats," *Veterinary Clinics of North America. Small Animal Practice* 33, no. 3 (2003): 533–552.

40. K. Batschinski, A. Nobre, E. Vargas-Mendez, et al., "Canine Visceral Hemangiosarcoma Treated With Surgery Alone or Surgery and Doxorubicin: 37 Cases (2005–2014)," *Canadian Veterinary Journal* 59 (2018): 967–972.

Supporting Information

Additional supporting information can be found online in the Supporting Information section. **Data S1:** Supporting Information. **Figure S1:** Establishment of canine HSA patient-derived xenograft (PDX) models. (A) Representative images of H&E staining and IHC for the endothelial markers CD31 and vWF. Images compare the original patient tumour with the corresponding PDX models. Insets show magnified views. Scale bars = 50 μm. (B) STR profiles of the established PDX models. **Table S1:** Antibody list. **Table S2:** Primer sequences for RT-qPCR. **Table S3:** Selected reference genes for qPCR. **Table S4:** sgRNA sequences. **Table S5:** Patient information of HSA PDX models.